ADVANCED MATERIALS
www.advmat.de

Regio-Selective Mechanical Enhancement of Polymer-Grafted Nanoparticle Composites via Light-Mediated Crosslinking

*Kyungtae Kim, Benjamin C. Grummon, Carl J. Thrasher, and Robert J. Macfarlane**

Polymer-brush-grafted nanoparticles (PGNPs) that can be covalently crosslinked post-processing enable the fabrication of mechanically robust and chemically stable polymer nanocomposites with high inorganic filler content. Modifying PGNP brushes to append UV-activated crosslinkers along the polymer chains would permit a modular crosslinking strategy applicable to a diverse range of nanocomposite compositions. Further, light-activated crosslinking reactions enable spatial control of crosslink density to program intentionally inhomogeneous mechanical responses. Here, a method of synthesizing composites using UV-crosslinkable brush-coated nanoparticles (referred to as UV-XNPs) is introduced that can be applied to various monomer compositions by incorporating photoinitiators into the polymer brushes. UV crosslinking of processed UV-XNP structures can increase their tensile modulus up to 15-fold without any noticeable alteration to their appearance or shape. By using photomasks to alter UV intensity across a sample, intentionally designed inhomogeneities in crosslink density result in predetermined anisotropic shape changes under strain. This unique capability of UV-XNP materials is applied to stiffness-patterned flexible electronic substrates that prevent the delamination of rigid components under deformation. The potential of UV-XNPs as functional, soft device components is further demonstrated by wearable devices that can be modified post-fabrication to customize their performance, permitting the ability to add functionality to existing device architectures.

1. Introduction

The addition of inorganic nanoscale fillers to soft polymer matrices is a general design strategy to achieve high-performance composites, as interactions between the filler and matrix phases can alter polymer chain motion or network structure.[1–6] Adjusting the shape, properties, or arrangement of fillers enables control over mechanical properties like hardness, fracture toughness, or fatigue resistance.[7–12] Inorganic nanoscale fillers can also add or modulate composite properties beyond the limited range of values easily attained with polymers alone, such as thermal conductivity,[13,14] electrical conductivity,[15] refractive index,[16] or dielectric constant.[17,18] However, when particle surfaces are not adequately compatible with the matrix,[19] filler aggregation leads to defects that decrease mechanical properties by acting as crack initiation or propagation sites[20] or reducing optical transparency due to light scattering.[21]

Polymer-brush-grafted nanoparticles (PGNPs)[22–24] are therefore an attractive means of producing composites with homogenous filler, particularly at high loading, as densely grafted polymer brushes provide steric hindrance that prevents filler aggregation regardless of inorganic volume fraction. Additionally, PGNPs can be more readily processed than free polymer brushes of the same composition, as PGNPs often have higher glass-transition temperature (T_g) or modulus (and thus can be more readily handled or shaped at ambient temperature).[25,26] Properties of PGNP composites can be modified by altering their polymer[27–29] and nanoparticle[30–33] compositions as well as the architecture of the PGNP[34–38] (e.g., grafting density, polymer length, particle size). While PGNP composites typically require long brush lengths to impart good mechanical strength, we have recently demonstrated that mechanical strength can also be achieved using short polymer brushes that can be post-synthetically crosslinked.[30,39,40] These crosslinkable polymer-grafted nanoparticles (XNPs) can achieve filler loadings as high as ≈82 wt.% while remaining easily processable before crosslinking and mechanically robust after. Although these prior XNPs

K. Kim, C. J. Thrasher, R. J. Macfarlane
Department of Materials Science and Engineering
Massachusetts Institute of Technology (MIT)
77 Massachusetts Avenue, Cambridge, MA 02139, USA
E-mail: rmacfarl@mit.edu
B. C. Grummon
Department of Chemistry
Massachusetts Institute of Technology (MIT)
77 Massachusetts Avenue, Cambridge, MA 02139, USA

The ORCID identification number(s) for the author(s) of this article can be found under https://doi.org/10.1002/adma.202410493

DOI: 10.1002/adma.202410493

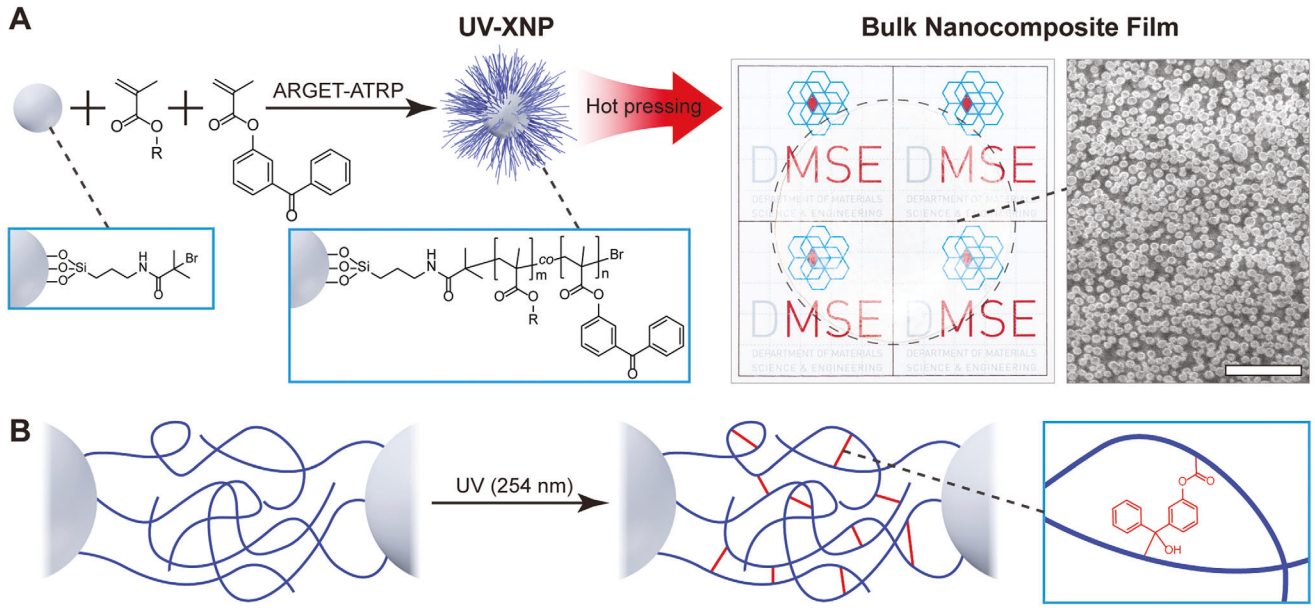

Scheme 1. A) Generalized synthesis and processing scheme for UV-XNP composite films. Optical image shows a demonstrative example of an ≈8 cm bulk nanocomposite film of PHMA UV-XNPs, with an inset FIB-SEM image demonstrating particle homogeneity within the sample. Bold grid in background of optical image: 5 cm. Scale bar in SEM image: 500 nm. B) Schematic illustration of UV-crosslinking of polymer brushes via photoinitiation of benzophenone pendant groups.

proved that forming covalent crosslinks during post-processing is a viable strategy for composite synthesis, their practicality in functional devices is hampered by the specific crosslinking chemistries that were used. Specifically, XNPs that used epoxide ring-opening chemistry to form crosslinks could only produce thin film coatings, and methacrylate-based XNPs that employed thermally-induced anhydride crosslinks exhibited both minor shrinkage and severe discoloration upon heat treatment. A more versatile crosslinking approach would enable XNPs to be used in synthesizing and fabricating composites for functional devices. Moreover, spatial control over crosslinking would potentially enable the synthesis of composites with tailored inhomogeneity in mechanical response, where select parts of the fabricated object could be made rigid or compliant as needed to adapt their use as structural or functional components of electronic, biomedical, or energy devices.[41–49]

Here we demonstrate a UV-mediated approach for crosslinking polymer-grafted nanoparticles (hereafter referred to as UV-XNPs) by incorporating UV-sensitive moieties within the PGNP brushes. A benzophenone-containing monomer is easily copolymerized with various monomers, thereby enabling a materials-versatile XNP synthesis approach. We show that the XNP architecture permits better processability of soft composites by increasing the viscosity of low T_g polymers, and benzophenone crosslinking drastically increases tensile modulus without altering the material's volume, shape, or optical clarity. Additionally, because these UV-active moieties are directly tethered to the PGNP brushes, UV light enables spatially-resolved control over crosslink density. This control allows for the formation of a crosslinked network where the mechanical response can be intentionally modified across a chemically homogenous composite. This advantage is demonstrated by grafting a simple electronic circuit to a PGNP-based soft substrate, where selective crosslinking of the substrate section to which the electronic components are attached allows for localized passivation of mechanical strain. As a result, the flexible substrate can be easily stretched, bent, or deformed without breaking the electrical circuit. Furthermore, the unique properties of UV-XNPs permit a new method of device fabrication and modification enabling modular device customization, which is rare in the field of stiffness-engineered materials for soft electronics.[50–52] UV-XNPs therefore present a significant advancement in the synthesis of complex polymer nanocomposites with high inorganic nanofiller content, and the fabrication of functional device components with deliberately designed inhomogeneous mechanical properties.

2. Results and Discussion

UV-XNPs were designed by grafting methacrylate-based copolymer brushes on silica nanoparticles, where small quantities of a methacrylate monomer containing a benzophenone moiety (4-benzoylphenyl methacrylate, BPMA) were incorporated into the polymer brush chains (**Scheme** 1A). Benzophenone is a photoinitiator that forms a radical after hydrogen abstraction when exposed to UV light (200–400 nm), and has been used for the crosslinking and curing process of polymeric materials.[53–56] Surface modification of silica nanoparticles of controlled sizes (50–60 nm, Figure S1, Supporting Information) was conducted by modifying the particle surfaces with atom transfer radical polymerization (ATRP) initiators, then using surface-initiated activators regenerated by electron transfer (SI-ARGET) ATRP to synthesize a random copolymer brush containing a methacrylate monomer and a pre-determined amount of BPMA.[57,58]

For initial experiments to demonstrate the UV-XNP concept, n-hexyl methacrylate (HMA) was used as the majority monomer due to the low glass transition temperature of PHMA homopolymer ($T_g \approx -5$ °C); the low T_g and rubbery nature of PHMA enables simple processing of the XNPs at modest temperatures.[39,59] We would note that although the T_g of PHMA is well below ambient temperature, the PGNP architecture reduces the fluidity of these materials, meaning that they are plastically deformed only when heated above ≈80 °C. This aspect of UV-XNPs is important for this work, as the use of a PGNP-based building block permits the composites examined herein to retain their shape under ambient conditions long enough to be processed and subsequently crosslinked. Thus, while benzophenone crosslinking has been used for polymer crosslinking previously, using a PGNP morphology is critical for ensuring that all UV-XNP compositions explored here can be easily molded or shaped prior to crosslinking.

A range of PHMA-based UV-XNPs were prepared containing different BPMA monomer fractions, polymer brush lengths, and particle core sizes; characterization of all materials is included in the supplementary information (Table S1, Figures S2, and S3, Supporting Information). Initial demonstrations of this concept were performed using a single PHMA UV-XNP (59 nm silica particle cores, with 43.4 wt.% silica and 6.4 wt.% BPMA monomers); subsequent experiments used additional compositions as noted in relevant sections below. Once synthesized, UV-XNPs were pressed at 150 °C to fabricate bulk nanocomposite films, then crosslinked with 254 nm UV light (Scheme 1B). To ensure that samples were fully crosslinked through the entire width of the film, the films were flipped halfway through the irradiation time.

The crosslinking of the PHMA UV-XNP nanocomposite films resulted in striking changes in their mechanical and chemical properties (**Figure 1A**). As a representative example, a non-crosslinked PHMA UV-XNP film was initially elastic, easily deformable, and stretchable without cracking (Movie S1, Supporting Information). When this film was immersed in THF (a good solvent for the P(HMA-*co*-BPMA) brush copolymer), it completely dissolved, forming a cloudy solution of dispersed PHMA UV-XNPs. However, after 24 h of UV irradiation, the film was significantly stiffer, resisting deformation and fracturing under stress instead of stretching or bending (Movie S1, Supporting Information). Additionally, the crosslinked PHMA UV-XNP film did not dissolve when immersed in THF; instead, it showed slight swelling while retaining its shape. In comparison, control nanocomposites consisting of pure PHMA-grafted nanoparticles (with the same particle core sizes and polymer brush composition, but lacking benzophenone moieties) showed no change in mechanical or chemical properties upon UV irradiation (Figure S4 and Movie S1, Supporting Information), indicating that the dramatic shift in mechanical and chemical properties of PHMA UV-XNP nanocomposites can be attributed to the photocrosslinking of BPMA within the polymer matrix.

As further confirmation of crosslinking, the IR absorption peaks between 1600 and 1700 cm^{-1} (which correspond to the benzophenone[60]) completely disappeared after UV irradiation (Figure 1B). Additionally, the non-crosslinked PHMA UV-XNP film showed the characteristic absorbance peak of BPMA at 332 nm, which did not exist in the film of pure PHMA-grafted nanoparticles (Figure 1C). Upon UV irradiation, the film's absorption at 300–400 nm initially increased after ≈3 h of irradiation, then decreased to absorbance values below those of the initial sample. This unusual absorbance behavior can be attributed to the formation of transient species produced as intermediates in the benzophenone radical crosslinking reaction.[54,61] A thorough investigation of crosslinking kinetics based on film thickness was also conducted, permitting characterization of the

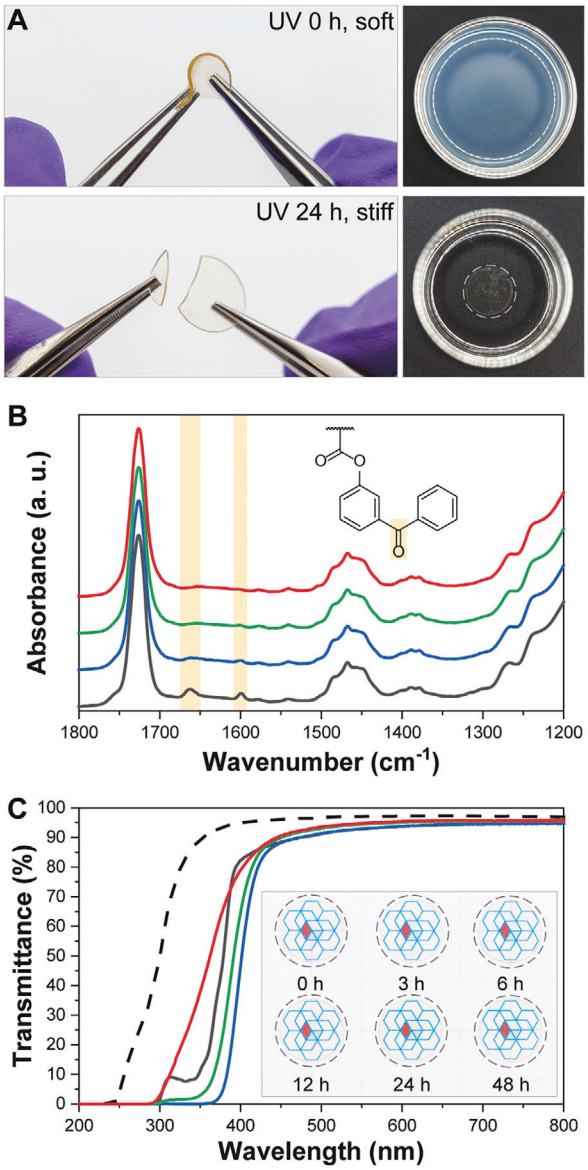

Figure 1. Characterization of photocrosslinking in PHMA UV-XNP composites. A) Composites exhibit different mechanical properties (left) and solubility in THF (right) before and after crosslinking. B) FT-IR data, demonstrating the reduction in benzophenone absorption modes after UV irradiation. C) Transmittance measurements of a film with 0.30 mm thickness. Black, blue, green, and red solid lines in B and C correspond to UV exposure times of 0, 3, 6, and 12 h, respectively. The dashed black line in C corresponds to PHMA-grafted nanoparticles that do not possess any benzophenone groups. Inset in C shows PHMA UV-XNP pellets (12 mm in diameter and 0.5 mm in thickness) at different UV exposure times. Grid: 10 mm.

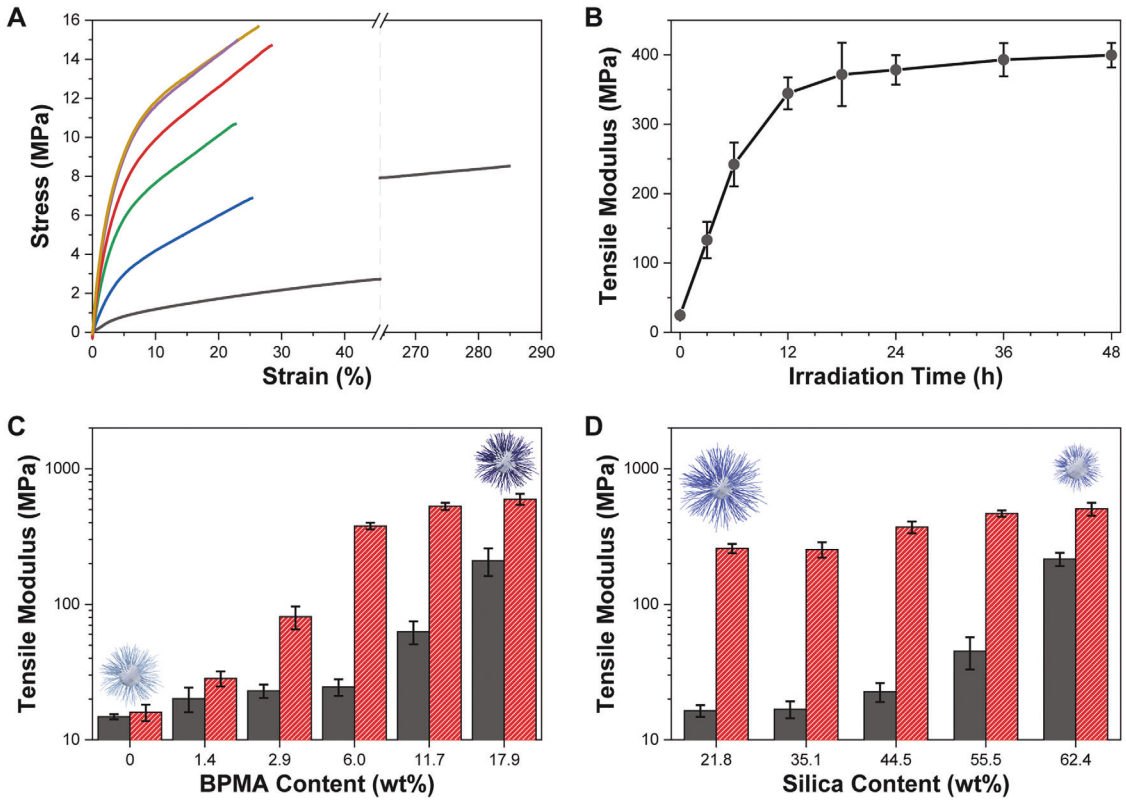

Figure 2. Mechanical properties of PHMA UV-XNPs. A) Representative stress-strain curves and B) tensile moduli of PHMA UV-XNP films with 46.0 wt.% silica and 6.0 wt.% of BPMA at different UV exposure times. C, D) Tensile moduli of different PHMA UV-XNP structures. Black, blue, green, red, purple, and gold lines in A correspond to UV exposure times of 0, 3, 6, 12, 24, and 48 h, respectively. The black and red bars in C and D correspond to UV exposure times of 0 and 24 h, respectively.

rates of UV-induced crosslink formation (Figure S6, Supporting Information).

Importantly, the samples remained entirely transparent to the eye throughout the crosslinking process, and no discernible deformation or distortion was observed in the films after UV irradiation (Figure 1C, **inset**). Quantitative analyses revealed statistically insignificant amounts of sample mass loss or shape deformation (Table S2, Supporting Information), and the microstructure of crosslinked nanocomposite films did not show the formation of any voids, defects, or aggregates of particles either before or after UV irradiation (Scheme 1A; Figure S7, Supporting Information). Collectively, these data demonstrate that the benzophenone moieties crosslink the UV-XNP composites without inducing any micro- or macroscopically observable alterations to material structure.

Tensile testing of UV-XNP materials more quantitatively demonstrates the remarkable shift in mechanical properties before and after crosslinking. For example, non-crosslinked PHMA UV-XNP films with 46.0 wt.% silica and 6.0 wt.% of BPMA were easily stretched (failure at ≈270% strain) with a tensile modulus of ≈24.5 MPa (**Figure** 2A; Figure S8, Supporting Information). Exposure to UV light caused large tensile modulus enhancement in the first ≈12 h of irradiation, with modest enhancement thereafter, up to ≈48 h of UV exposure (Figure 2B). These UV-XNPs ultimately reached a maximum tensile modulus of ≈400 MPa, more than an order of magnitude difference in modulus compared with the non-crosslinked sample (Table S3, Supporting Information). The toughness of the PHMA UV-XNP film sharply decreased after UV irradiation because of a loss of elasticity (≈30% maximum strain), likely due to the crosslinks reducing the relaxation of physically entangled polymer chains (Figure S14, Supporting Information).

Using this initial UV-XNP design as a baseline, a series of PHMA UV-XNPs with varying amounts of BPMA, silica content, and filler particle size were examined to explore how alterations to UV-XNP composition affect the crosslinking process and subsequent mechanical performance. At a fixed particle size and polymer brush length, the tensile moduli of all non-crosslinked PHMA UV-XNP samples with less than 6.0 wt.% BPMA were between 20 and 25 MPa, similar to the modulus of pure PHMA-grafted nanoparticles (≈14.8 MPa, Figure 2C). PHMA UV-XNP composites with >12 wt.% BPMA were glassy and cracked easily when deformed, as PBPMA has a higher T_g (≈118 °C).[60] After crosslinking, the tensile moduli of the samples increased concomitantly with the amount of BPMA, with the largest enhancement at 6.0 wt.% BPMA—a 15.4-fold change after UV exposure (Table S4, Supporting Information). The lowest initial amount of BPMA tested using PHMA UV-XNP composites was 0.03 wt.%, which showed no mechanical enhancement upon crosslinking (Table S4, Supporting Information). However, even these minimally crosslinked films only swelled in THF and did not dissolve, indicating that at least some crosslinking had occurred.

(Figure S4, Supporting Information). The gelation of PHMA UV-XNPs at extremely low amounts of crosslinker highlights an additional important advantage of the PGNP architecture, as grafting a large number of polymer chains to a common nanoparticle core allows the particle to effectively act as a "node" that allows for a fully percolating network to be formed with minimal UV-induced crosslinks between polymer chains.[62] The crosslinking-induced mechanical enhancement of PHMA UV-XNPs with higher than 11.7 wt.% of BPMA was somewhat small compared to the enhancement rate of those with lower than 6.0 wt.%, which we attribute to the moderately glassy character of the non-crosslinked polymer. It is also possible that UV penetration and crosslinking efficiency inside the film would be lower with increasing BPMA content due to absorption from both the BPMA and the transient species formed upon irradiation (as discussed previously).

By altering the length of the PHMA brushes, PHMA UV-XNP inorganic content could be varied from 21.8 to 62.4 wt.% (for all samples, BPMA content ≈6 wt.%), resulting in significant changes to mechanical properties (Figure 2D). When modulating polymer brush height, a consistent rate of mechanical enhancement was observed across UV-XNP films that contained less than 44.5 wt.% silica content (Table S5, Supporting Information), in accordance with the fact that this range of polymer brush heights all exist within the semi-dilute brush regime, as supported by the calculated grafting density (Table S1, Supporting Information), and readily entangle.[36,38,63] This observation was consistent with PHMA UV-XNPs with ≈45 wt.% of silica but different core sizes (Table S6, Supporting Information). When silica content increased beyond 45 wt.%, however, the entropic penalty of dense, elongated polymer brushes prohibited sufficient entanglement. Thus, while the final crosslinked materials had similar moduli, the initial materials were stiffer and more difficult to process.

An important advantage of UV-XNPs is the ability to copolymerize the BPMA with other monomers, thereby enabling a versatile and modular approach for synthesizing and processing composites with a wide range of mechanical, chemical, and physical properties. To demonstrate this concept, a series of UV-XNPs were prepared consisting of random copolymers of BPMA and one of multiple other monomers: methyl methacrylate (MMA), ethyl methacrylate (EMA), n-butyl methacrylate (nBMA), lauryl methacrylate (LMA), i-butyl methacrylate (iBMA), tert-butyl methacrylate (tBMA), cyclohexyl methacrylate (cHMA), 2-ethyl hexyl methacrylate (2EHMA), benzyl methacrylate (BzMA), 2-hydroxy ethyl methacrylate (HEMA), 2-(dimethylamino)ethyl methacrylate (DMAEMA), 2,2,2-trifluoroethyl methacrylate (TFEMA), poly(ethylene glycol) methacrylate having a number-average molecular weight (M_n) of 360 g mol^{-1} ($PEG_{360}MA$), poly(ethylene glycol) methyl ether methacrylate having an M_n of 300 g mol^{-1}, ($PEG_{300m}MA$) and 500 g mol^{-1}, ($PEG_{500m}MA$), t-butyl acrylate (tBA), n-hexyl acrylate (HA), and styrene (**Figure 3A**). Importantly, each of these UV-XNPs was prepared and processed with only slight modification to the PHMA UV-XNP synthetic protocol, indicating the adaptability of this composite fabrication strategy.

After UV-XNP synthesis and characterization (Table S7 and Figure S15, Supporting Information), all samples were irradiated with UV light and immersed in solvent to verify crosslinking (Figure 3B; Figure S16, Supporting Information). For all UV-XNP compositions, the non-irradiated UV-XNP films readily dissolved in good solvents for their respective monomers. Conversely, all crosslinked films remained solid, even those made from UV-absorbent monomers (BzMA and styrene) that could not be fully crosslinked (Figures S17 and S18, Supporting Information). Moreover, these films exhibited different degrees of swelling when immersed in different solvents, consistent with the expected solubility of their neat copolymer brushes (Figure 3B, enlarged images in Figure S19, Supporting Information). These results indicate that the chemical properties and stability of UV-XNPs can be easily tailored for use in applications that require hydrophobic, hydrophilic, or fluorophilic environments, and can also be modified to include reactive groups (e.g., amines) that can be further modified by post-processing. In addition to their dissimilar chemical properties, the mechanical responses of these UV-XNPs with different polymer compositions were also distinct. For example, unlike the soft and flexible behavior of PHMA UV-XNPs ($T_g \approx -5$ °C), PMMA and PHEMA UV-XNPs were glassy and rigid regardless of crosslinking due to their high T_g (≈105 °C for PMMA, ≈87 °C for PHEMA).[64,65] Again, it is important to note that the use of brush particles enabled these behaviors (vide supra), as BPMA random copolymers often require a higher degree of crosslinking to achieve a fully connected polymer network and mechanical enhancement. Further, these materials are much more processable than the neat copolymers before crosslinking, as discussed previously.

Importantly, the PHMA UV-XNP nanocomposites constitute a free-standing, solvent-free material, with the crosslinkable benzophenone groups covalently bound to the polymer brushes. Thus, the active crosslinking species cannot diffuse away from the sites where photoinitiation occurs, which permits regioselective crosslinking through spatial control of UV irradiation. This design parameter could therefore potentially enable the formation of macroscopic solids with continuous network connectivity and homogenous material composition but intentionally anisotropic mechanical responses. The feasibility of this stiffness patterning concept was examined directly by blocking the UV exposure to selective areas of a PHMA UV-XNP film via a UV-opaque masking layer of adhesive vinyl film (**Figure 4A**, **top**).

As seen in earlier studies, photocrosslinking did not cause any deformation or noticeable changes in the film, leaving unmasked domains indistinguishable from adjacent masked domains when the films were at rest (Figure 4A, **bottom left**). However, when the films were stretched, non-uniform elongation was observed—the UV-irradiated "hard" regions of the materials retained their shape, while the adjacent "soft" regions that were masked easily elongated, exhibiting necking behavior at their interface (gray dashed lines show sample profile). To visualize these different mechanical behaviors more effectively, stress distribution within the films was monitored using a cross-polarized lighting setup, as the photoelastic behavior of polymeric materials produces birefringence when deformed.[66] At rest, the non-stretched films appeared homogeneously transparent regardless of lighting setup, but as the films were strained, the non-crosslinked regions exhibited a pale blue color while the crosslinked regions remained transparent (Movie S2, Supporting Information). These different optical behaviors clearly show which portions of the sample were irradiated and crosslinked, and demonstrate that localized crosslinking did not induce any internal stresses.

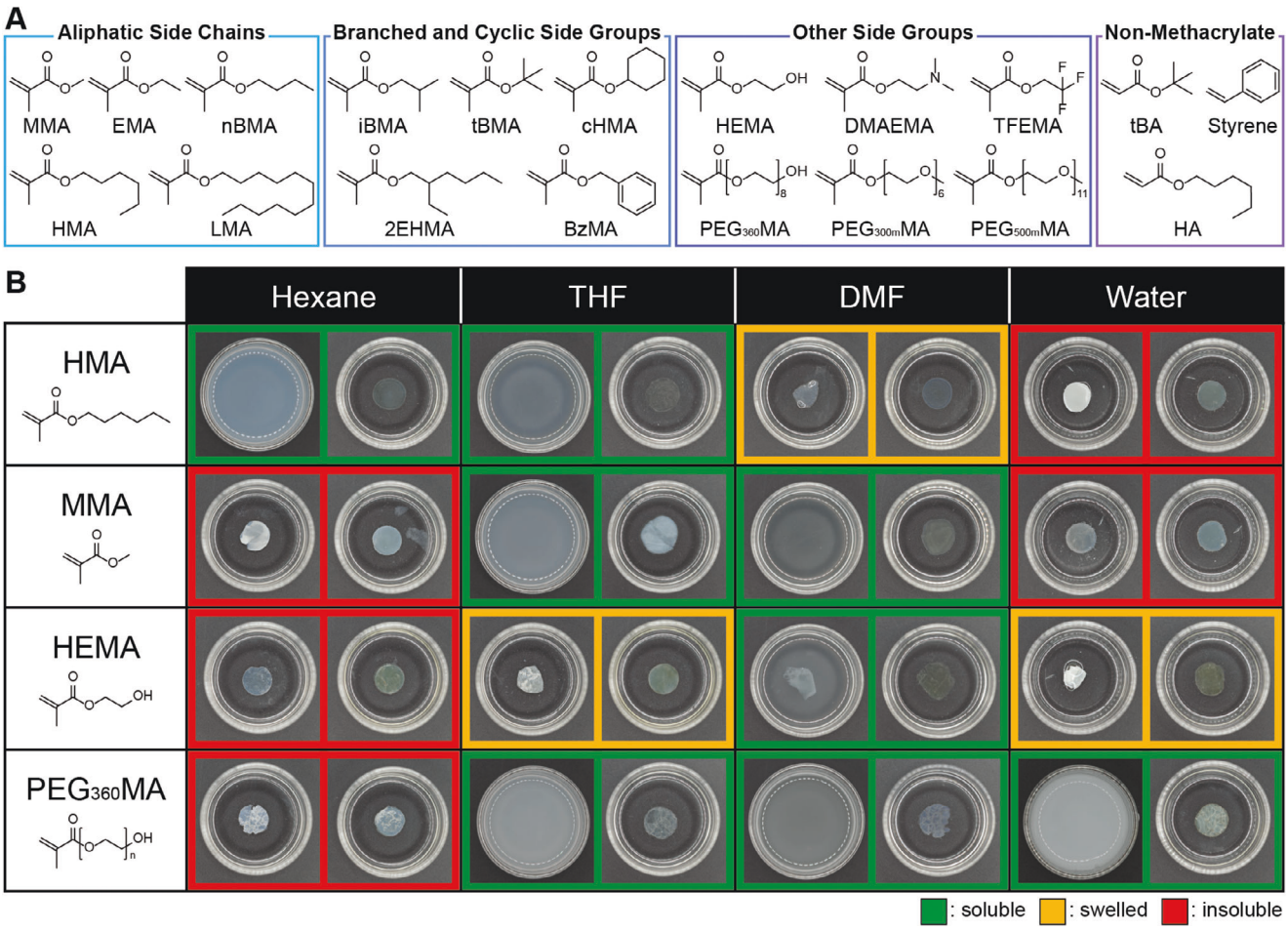

Figure 3. A) Monomers used to form UV-XNP polymer brushes. B) Stability and swelling tests of UV-XNPs in various solvents before (left) and after (right) photocrosslinking, demonstrating that all UV-XNP compositions can indeed be crosslinked. The relative solubilities of the UV-XNPs match the expected solubilities of their corresponding polymer compositions, indicating that the incorporation of BPMA does not significantly alter the chemical properties of the base polymer used as a UV-XNP brush. Pellet diameter: 10 mm.

Using the initial sample with just one crosslinked domain (Figure 4A, **bottom left**), the local strain within the hard domain was measured to be ≈6%, significantly lower than the 50% global strain that was applied. In contrast, the upper and bottom soft domains were elongated to ≈88% and ≈56%, respectively, indicating that the strain was almost exclusively located in the soft domains, and the hard domains were passivated from the strain. The uneven stretching of upper and bottom soft domains is attributed to inherent defects of the film testing setup (i.e., non-identical gripping fixtures).

The soft domains of these masked films could also be irradiated multiple times to introduce further complexity in their mechanical response (Figure 4B, full details of procedure depicted in Figure S20, Supporting Information). The direct correlation between the amount of UV-light exposure and the stiffness of the films permits the intentional design of continuously connected and compositionally homogeneous materials that can be intentionally engineered with inhomogeneous mechanical properties, including both regions of high contrast in stiffness and gradient materials with gradual changes in modulus across a sample (Figure 4C; Figure S22 and Movie S2, Supporting Information). The use of UV-induced crosslinking can even produce stiff regions with complex shapes by designing masks with specifically shaped cutouts (Figure 4D; Movie S2, Supporting Information). For example, the resolution of the crosslinking process was sufficiently high to introduce features such as the vertices of hexagon and star shapes, as well as small gaps between features (gaps between the three circle features in Figure 4D are 0.5 mm). More complex patterns, such as a "windshield frit" gradient-dotted pattern with a minimum diameter of 1.3 mm, and the MIT logo having anisotropy with respect to the elongation direction, further demonstrate the versatility of this approach. It should also be noted that in all cases, the crosslinked regions are undetectable prior to stretching or when not under cross-polarized illumination (Figure S21, Supporting Information).

In addition to their compositional versatility, a unique advantage provided by UV-XNPs for composite fabrication is the ability to formulate materials that have a consistent chemical composition and physical appearance, but locally tailored mechanical response. This combination of properties is desirable for structures that have specifically tailored failure modes,[67,68] or complex soft devices that need to deform globally while

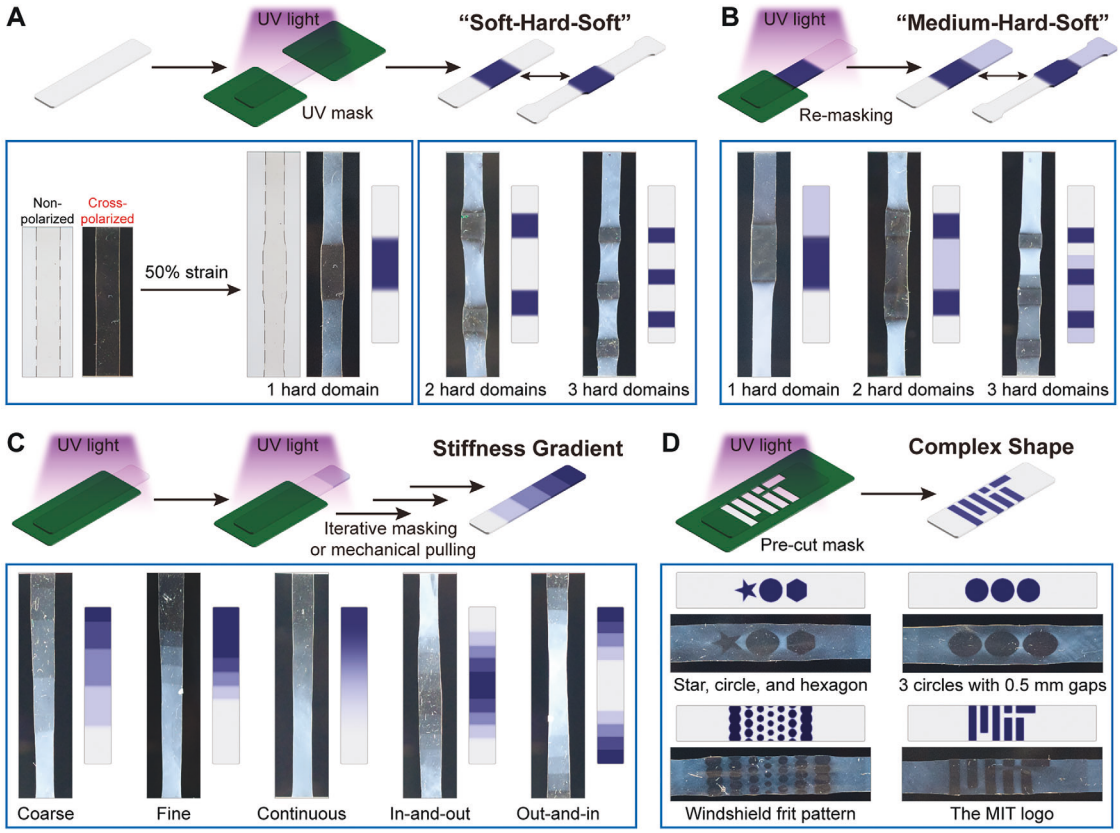

Figure 4. UV masking of PHMA UV-XNP nanocomposite films. A) Single-step patterning of "hard" and "soft" domains, where only UV-irradiated regions of the sample are crosslinked. Under non-polarized light, both hard and soft domains are equally transparent with no obvious differences in appearance. Under cross-polarized light, strained regions of the sample become birefringent, permitting observation of strained (non-crosslinked, light blue regions) and passivated (crosslinked, dark blue regions). B) Two-step tertiary stiffness domain patterning, where the amount of crosslinking is controlled as a function of irradiation time. The gradient of light to dark blue color indicates relative stiffness. C) Stiffness gradient patterning via multiple rounds of UV irradiation where the mask was moved after each round, or via continuous moving of the mask during irradiation. D) Pre-designed complex shape patterning through photomasking select regions of the samples. A diagram of the pattern design is shown above the cross-polarized light image of each sample. Length of the photos of stretched films: 45 mm (A to C) and 48 mm (D).

retaining specific local features.[41] Examples include wearable electronics,[42,43] mechanical sensors,[44] and soft robotics.[69] As a simple proof-of-concept device to demonstrate UV-XNPs' future applicability to these technologies, a flexible electronic substrate was fabricated with PHMA UV-XNP with 21.8 wt.% silica content and 6.2 wt.% of BPMA. Micro-LEDs were adhered to two PHMA UV-XNP films—a sample that was locally crosslinked in the region to which the LED was attached and a compositionally identical control sample that was not crosslinked. LEDs were placed on these samples using epoxy adhesive (while ensuring that leads did not adhere to the substrate), and stretchable electronic wires were drawn across the PHMA UV-XNP substrates using eutectic gallium-indium (EGaIn).

When stretching and bending the crosslinked substrate, the junction between the LED and liquid metal wire remained intact, indicating that the crosslinking successfully passivated local strain underneath the LED (**Figure** 5A). Thus, even though the LED leads were not directly adhered to the substrate, the local structure of the circuit was preserved while permitting the overall device to be deformed. Conversely, the non-crosslinked substrate caused a break in the circuit where the liquid metal contacted the LED leads when stretched or bent. (Figure 5B). The ability to intentionally generate localized stiff domains in a flexible composite significantly benefits soft substrates by reducing the need for conductive epoxies for component adhesion and by providing additional mechanical support around junctions between electrical leads and other components where circuit breaks are most likely to occur.

One of the unique advantages of UV-XNP composites as a soft substrate for flexible electronics is that the substrate film can be post-crosslinked selectively at sites where rigid components are mounted, resulting in component-oriented strain passivation. This ensures that the hard and rigid device components remain connected to the substrate during mechanical deformation and device operation. Moreover, because the UV-XNP architecture allows the substrate material to maintain a consistent shape before being crosslinked, the location of electronic components can be placed, adjusted, and customized without any restrictions on substrate or circuit design. To demonstrate the utility of this advantage that UV-XNP-based flexible materials possess, three rectangular substrates of PHMA UV-XNPs with identical dimensions

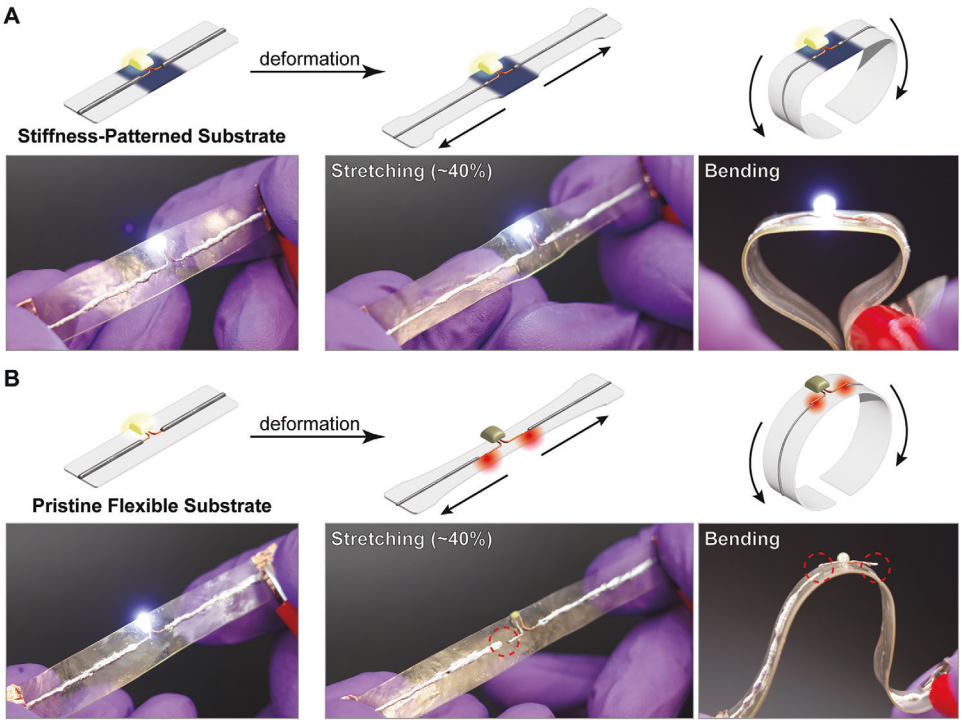

Figure 5. Flexible electronic substrates made from PHMA UV-XNP composites. Micro-LEDs are adhered to the substrate and connected to a power source via stretchable wires composed of EGaIn. A) Crosslinking the substrate underneath the micro-LED allows the circuit to be stretched or bent without breaking connectivity. B) In a non-crosslinked sample, without the rigid domain around micro-LED, the circuit easily breaks when the substrate is deformed.

were prepared, and three red micro-LED chips were mounted to each of these non-crosslinked substrates at distinct locations. (**Figure** 6A, **left**). To form crosslinked domains around the device components, masking films with oval-shaped holes corresponding to the location and size of the LEDs were designed. Notably, the substrates were irradiated from behind (i.e., the mask and UV source were placed on the side opposite the LEDs) to ensure the LEDs would not hinder substrate crosslinking by scattering or blocking the UV light. When the substrates were stretched after crosslinking, transparent oval-shaped "hard" domains around the LEDs were observed under cross-polarized light, while the rest of the substrate remained flexible (Figure 6A, **middle**). Liquid metal wires were then drawn to connect the LEDs to a power source, resulting in stretchable circuits with no constraints on the position of electrical components (Figure 6A, **right**). Moreover, the initial substrates were compositionally identical and did not possess any pre-determined crosslinked domains, indicating that UV-XNPs permit the simple fabrication of customizable flexible substrates without the need for complex processing tools or methods.

Importantly, since UV-XNP nanocomposites can be fabricated into a freestanding film prior to crosslinking, a flexible wearable device can even be directly fitted to the intended user—the necessary device shape and component positions can be marked on the initial substrate as it is interfacing with the intended user before device fabrication (Figure 6B). To demonstrate this concept, a layout of a fingertip pressure sensing device for an index finger was determined from the master blueprint of the device after direct fitting on the user's hand (Figure 6C; Figures S23, and S24, Supporting Information). Based on the fitting, the customized sensing device that exactly fit to the user's index finger was fabricated (Figure 6D). Despite the pressure sensor being mounted to a curved fingertip, and exposed to external stress whenever touching a surface, the LED on the signal section of the device turned on successfully, indicating that the sensor leads were isolated from the typical stresses of device usage (Figure 6E). Further evidence of the customizability of this approach was shown by fabricating separate devices attached to different templates (e.g., a thumb instead of an index finger, Figure S25, and smaller fingers, Figure S26, Supporting Information). These demonstrations show that UV-XNP nanocomposites are a powerful tool for customizing soft electronics while maintaining their basic circuit components and layout.

Finally, the simplicity of this fabrication approach, which permits multiple rounds of UV-crosslinking to tailor stiffness (Figure 4), also permits post-fabrication customization to modify existing flexible devices without disrupting device function. Adding additional stiffness patterns to pre-patterned substrates is potentially impactful for the field of soft electronics because it enables pre-existing circuits to be further modified, upgraded, or repaired.

As a proof-of-concept for the post-modification of soft electronic devices using UV-XNP composites, a multifunctional thermal and pressure sensing device was produced from the layout of the pressure sensing device made previously (**Figure** 7A). A new device was fabricated and tested in the same manner as before to verify its function as a pressure sensor (Figure S27, Supporting Information). Having successfully tested the device's operation,

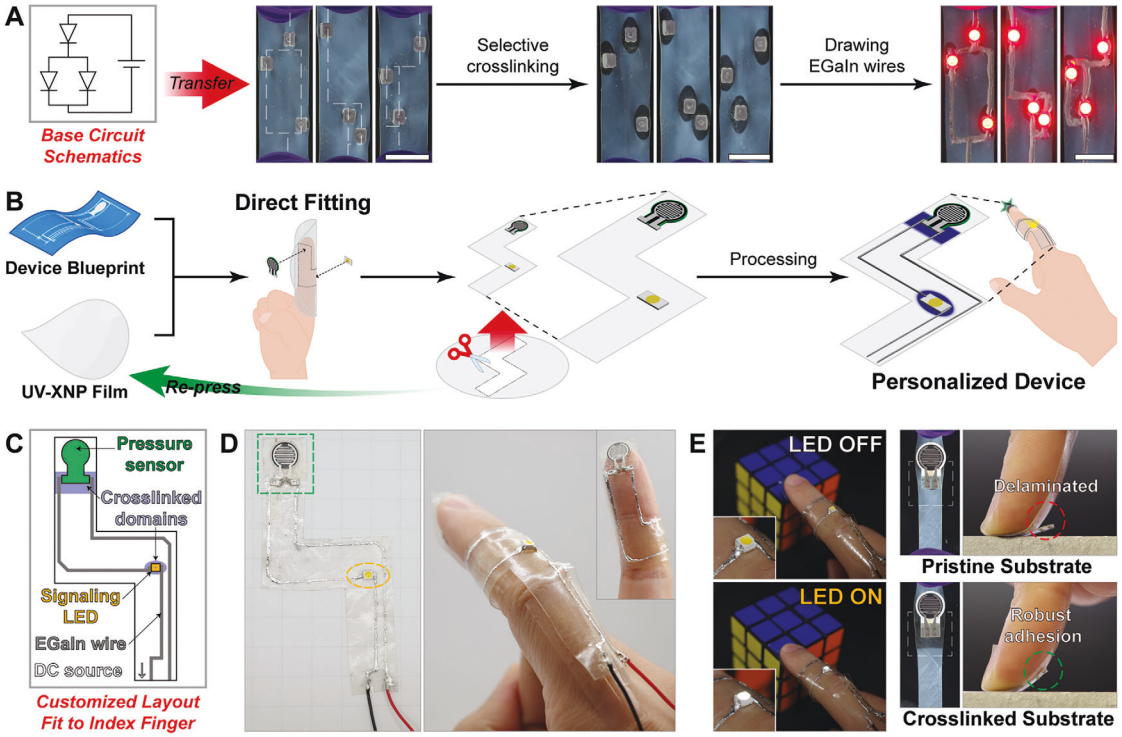

Figure 6. Component-oriented crosslinking of stiff domains on a flexible electronic substrate A) Micro-LEDs are positioned arbitrarily on three identical substrates, then irradiated with masks to selectively crosslink the substrate underneath the LEDs. After connecting circuits with EGaIn wires, substrates can be stretched without breaking the patterned circuits. Scale bar: 10 mm. B) Fabrication of a personalized, customizable pressure sensing device via direct fitting on the wearer's hand. C) Layout of the custom-sized fingertip pressure sensing device. D) Fabricated device containing a pressure sensor (green dashed box) and a white LED (yellow dashed circle). Grid: 10 mm. E) Demonstration of pressure sensing and prevention of delamination upon device stretching.

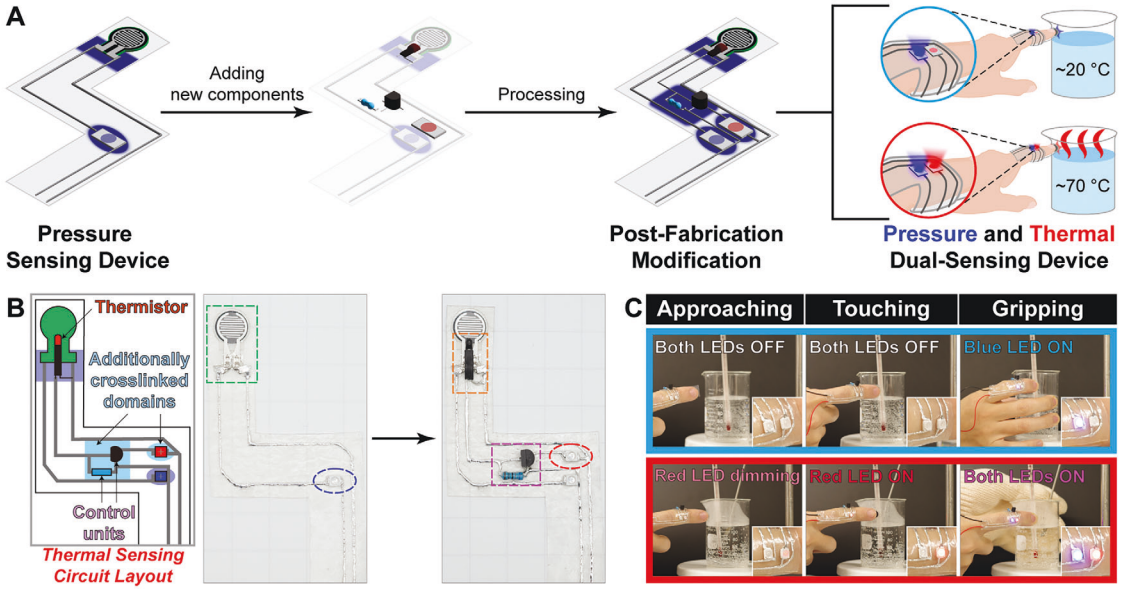

Figure 7. Post-modification of customized, modular devices using PHMA UV-XNP nanocomposite. A) A fully functional pressure sensing device is further modified into a thermal and pressure dual-sensing device by adding new components for thermal sensing circuit and further crosslinking the substrate. B) Schematic for the thermal sensing circuit overlaid on the pre-existing device, containing a pressure sensor (green dashed box) and a blue LED (blue dashed circle) for signaling, a thermistor (orange dashed box), resistor, transistor (pink dashed box), and red LED (red dashed circle). Liquid metal wires are drawn to complete the new circuit. Grid: 10 mm. C) The post-modified dual sensing device successfully functions when the targeted stimuli are applied. Blue box and red box indicate the temperature of the beaker at ≈20 °C and ≈70 °C.

a thermal sensing circuit was added by incorporating four additional electronic components (Figure 7B; Figures S23, and S24, Supporting Information). The functionality of this dual-sensor device was then tested to verify that the initial pressure-sensing circuit and the newly added thermal-sensing circuit could still both function on the flexible substrate (Figure 7C). At ambient temperature, the blue LED of the pressure sensor was activated upon contact with a room-temperature beaker, but the red LED of the thermal sensor remained inactive. In contrast, when approaching a hot surface (a beaker filled with ≈70 °C water), the red LED was dimly lit, and fully lit when touching the hot surface, providing feedback on the thermal environment around the device. Additionally, the blue LED of the pressure sensor turned on when the surface was pressed, showing the two components operated independently, and the addition of the thermal sensor did not impair the function of the pressure sensor.

3. Conclusion

The UV-mediated crosslinking of XNP composites presented in this work provides a versatile, controllable, and simple method to create mechanically transformable and mechanically anisotropic nanocomposites with well-dispersed and highly-filled inorganic filler content. The photocrosslinking mechanism of benzophenone moieties allows various design handles within the architecture of UV-XNPs, such as copolymer composition, amount of crosslinker, filler content, and polymer length, enabling both broad and targeted tuning of mechanical and chemical properties of UV-XNP composites. Importantly, the photocrosslinking of UV-XNPs is a conservative process and results in no deformation nor discoloration of UV-XNP composites upon crosslinking, which circumvents previous limitations in XNP design, thereby allowing the exploration of XNP composites in optical and photonic applications. Furthermore, spatial control over a nanocomposite's mechanical properties is paramount in fields with large demands on stiffness-patternable soft materials. This work further demonstrates not only the ability to spatially control crosslinking in XNP composites but also the potential of these materials as stiffness-patterned flexible electronic substrates with a totally new method of device fabrication. Thus, UV-XNPs achieve significant improvements on previous PGNP composites toward applications across a variety of fields. As functional materials with a unique set of material properties, UV-XNPs provide a new, generalizable design platform for chemically and mechanically diverse nanocomposites.

4. Experimental Section

Materials: *N,N*-dimethylformamide (DMF, anhydrous, 99.8%) and methyl methacrylate (MMA, 99%) were purchased from Acros Organics. Tris[2-(dimethylamino)ethyl]amine (Me_6TREN, 98%+) and n-hexyl acrylate (HA, 95%) were purchased from Alfa Aesar. 4-benzoylphenyl methacrylate (BPMA, 98%) was purchased from Ambeed Inc. Ammonium hydroxide (28.0 to 30.0% in water) was purchased from Fisher Chemical. 200 proof pure ethanol was purchased from Koptec. Anisole, (≥99.0%), α-bromoisobutyryl bromide (98%), benzyl methacrylate (BzMA, 96%), copper(II) bromide (99%), 2-(dimethylamino)ethyl methacrylate (DMAEMA, 98%), hydrofluoric acid (48% in water), 2-hydroxyethyl methacrylate (HEMA, ≥99%), lauryl methacrylate (LMA, 96%), poly(ethylene glycol) methacrylate having an M_n of 360 g mol^{-1} (PEG_{360}MA), poly(ethylene glycol) methyl ether methacrylate having an M_n of 300 g mol^{-1} (PEG_{300m}MA) and 500 g mol^{-1} (PEG_{500m}MA), styrene (≥99%), tert-butyl acrylate (tBA, 98%), tert-butyl methacrylate (tBMA, 98%), triethylamine (≥99.5%), and 2,2,2-trifluoroethyl methacrylate (TFEMA, 99%) were purchased from Sigma Aldrich. Cyclohexyl methacrylate (cHMA, 98.0+%), 2-ethylhexyl methacrylate (2EHMA, 99.0+%), ethyl methacrylate (EMA, 99%), and n-hexyl methacrylate (HMA, 98.0+%) were purchased from TCI America. (3-Aminopropyl)triethoxysilane (99%), eutectic gallium-indium (99.99%), i-butyl methacrylate (iBMA, 99%), n-butyl methacrylate (nBMA, 99%), tetraethoxysilane (99.90%), and tin(II) 2-ethylhexanoate (95%) were purchased from Thermo Scientific Chemicals. General solvents were purchased from Fisher Scientific. Monomers were filtered through a short column of basic alumina to remove the inhibitor prior to polymerization. All other chemicals were used as received.

Synthesis and Surface Modification of Silica Nanoparticles: Silica nanoparticles were prepared via the Stöber method using a slightly modified procedure that was reported previously.[39,40] In a standard synthesis of ≈60 nm diameter nanoparticles, 200 proof ethanol (1325 mL), ammonium hydroxide (28.0 to 30.0% in water, 80 mL), and deionized water (39 mL) were combined in a two-neck 2 L round-bottom flask with a magnetic stir bar and a glass stopper. The flask was then placed on a heating mantle with a thermocouple connected to a temperature controller. The solution was heated to 60 °C and stirred for 1 h. Once the temperature stabilized, tetraethoxysilane (57 mL) was added quickly into the solution while stirring at 300 rpm. When the solution became homogeneous after a few seconds, the stirring rate was reduced to 150 rpm, and the reaction continued for 3 h. Afterward, the cloudy white solution of silica nanoparticles was collected, washed, and centrifuged with ethanol and toluene for 3 cycles, respectively. All the resulting dispersions were transferred into a 250 mL round-bottom flask with a stir bar, and additional toluene was added until the total volume became ≈150 mL. The flask was sealed with a rubber septum, purged with nitrogen, and placed in an oil bath at 85 °C for 30 min. Then, 600 µL of (3-aminopropyl)triethoxysilane in 3 mL of toluene was injected quickly into the dispersion under vigorous stirring. After 3 h, the flask was cooled in an ice-water bath. When the dispersion was completely cool, 800 µL of triethylamine was added. Subsequently, 800 µL of α-bromoisobutyryl bromide in 8 mL of toluene was added dropwise under vigorous stirring. After 30 min, the ice-water bath was removed, and the reaction was allowed to proceed overnight. The surface-modified silica nanoparticles were purified through washing with centrifugation: Three times in a water/acetone (1:2 v v^{-1}) mixture, once in acetone, and finally three times in anisole. The particles were then dispersed in ≈100 mL of anisole and kept in a freezer. The wt.% concentration of the resulting stock solution was ≈18 wt.% silica in anisole, calculated with gravimetric analysis. The solution was later used for surface-initiated polymerization.

Synthesis of PHMA UV-XNPs: All UV-XNPs were synthesized by surface-initiated polymerization on silica nanoparticles using activators regenerated by electron transfer atom transfer radical polymerization (ARGET-ATRP). For a typical large-scale synthesis of PHMA UV-XNPs targeting ≈45 wt.% silica content, 48 g of silica nanoparticle stock solution in anisole diluted to 6.25 wt.% (3 g of silica nanoparticles), 4.5 g of a HMA solution containing 6 wt.% of BPMA, and 0.5 g of $CuBr_2$/Me_6TREN stock solution in DMF (2 mg of $CuBr_2$, 6 µL of Me_6TREN in 1 g of DMF) were mixed in a 100 mL round-bottom flask. The reaction mixture was purged with nitrogen, and 100 µL of tin(II) 2-ethylhexanoate in 1 g of anisole was injected into the reaction mixture. Subsequently, the flask was placed into an oil bath heated to 85 °C and stirred for over 12 h, allowing 80% monomer conversion. To purify PHMA UV-XNPs, the reaction mixture was dissolved in THF, followed by four cycles of centrifugation: three in THF and one in acetone. The resulting white precipitate was then dried under a vacuum for 1 day. To modify the structure of PHMA UV-XNPs, the BPMA concentration of the monomer mixture, the concentration of silica nanoparticle stock solution, or the size of silica nanoparticles could be varied.

Synthesis of Other Non-PHMA-Based UV-XNPs: UV-XNPs using MMA, EMA, nBMA, iBMA, LMA, and 2EHMA were synthesized according to the procedure of PHMA UV-XNPs described above after substituting HMA with the desired monomer and reducing the reaction scale (0.5 g of silica nanoparticles, 0.75 g of monomer mixture, 0.1 g of $CuBr_2$/Me_6TREN stock solution in DMF, 7.5 g of anisole, and 20 µL of tin(II) 2-ethylhexanoate).

For UV-XNPs using tBMA, BzMA, cHMA, DMAEMA, TFEMA, tBA, HA, and styrene, the monomer mixture and anisole amounts were adjusted to 2.5 and 5 g, respectively. When using $PEG_{360}MA$, $PEG_{300m}MA$, and $PEG_{500m}MA$, the monomer mixture and anisole amounts were adjusted to 1.5 and 5 g, respectively. When using HEMA, the amount of monomer mixture and anisole was adjusted to 5 and 2.5 g, respectively, and the resulting UV-XNPs were washed with ethanol instead of THF.

Hot Pressing of UV-XNPs: UV-XNP composite films were prepared by pressing on a Carver 4386 press at 150 °C between stainless-steel plates (0.80 mm in thickness) coated with fluorinated ethylene propylene film (Bytac) separated by a ring shim (0.1–0.5 mm thick). Samples were warmed in the press for 2 min prior to pressing, then pressed under a maximum load of ≈2000 kg. The press was water-cooled to room temperature for ≈15 min before removing the pressed samples. The resulting flexible disks were used as is with the desired diameter after removing them from the ring shim or cut into specific shapes using a razor blade or a round hole punch.

UV Curing: UV-XNP composite films and pellets were cured using a UVP CL-1000 Ultraviolet Crosslinker equipped with a 254 nm UV lamp with an intensity of ≈4 mW cm^{-2}. The temperature inside the chamber was held below 50 °C. Samples were placed on a mirror-finished stainless-steel substrate and cured for the desired time duration.

Focused Ion Beam Scanning Electron Microscopy (FIB-SEM): Cross-sectional micrographs were collected on the Helios Nanolab 600 Dual-Beam focused ion-beam milling system with a 52° relative difference between the ion and electron beam. To obtain FIB-SEM images, samples were first sputter coated with 30 nm of gold before using in the FIB-SEM. Samples were milled with a 6.5 nA (30 kV) Ga ion beam, after which the cross-section was cleaned with a 2.8 nA (30 kV) Ga ion beam. Each cross-section was imaged with an 86 pA (5 kV) electron beam using the in-lens detector on the scanning electron microscope without using the software's tilt correction.

UV-Vis Spectrometry and Transmittance Analysis: Transmittance measurements of PHMA UV-XNP films were performed on a Perkin Elmer Lambda 1050 UV/Vis/NIR Spectrophotometer equipped with a Three-Detector Module. A typical sample was prepared by pressing a PHMA UV-XNP film with a thickness of 0.5 mm onto a quartz substrate (25.4 mm × 25.4 mm × 1.59 mm) under a maximum load of ≈200 kg at 150 °C with subsequent water cooling. When crosslinking, the PHMA UV-XNP film was not flipped in the middle of the crosslinking time to allow for the interrogation of the crosslinking mechanism.

Fourier-Transform Infrared Spectroscopy (FT-IR) Analysis: FT-IR spectra were obtained on a Thermo Fisher Nicolet iS50 spectrometer equipped with an attenuated total reflection (ATR) accessory and a diamond window. A small piece of film with 0.5 mm in thickness was used, and data was collected from 4000–400 cm^{-1}, with 128 scans and automatic baseline and ATR correction.

Tensile Testing: Tensile tests were performed on a Zwick Roell Z010/TH system equipped with a 500 N load cell and polyurethane-lined screw grips, with an initial grip separation of 12 mm and separated at a rate of 50% strain per minute (6 mm min^{-1}). Samples of dimensions 25 mm × 2.5 mm × 0.6 mm were cut from pressed nanocomposite films using parallel razor blades before curing and used for tensile testing. To ensure the samples remained flat and straight, both ends of each sample were fixed in place with double-sided adhesive tape during crosslinking. Tensile modulus was determined by a linear fit between 0.05 and 0.25% strain, and tensile modulus and toughness were averaged across five samples.

Solubility and Swelling Test: Pellets of UV-XNPs (10 mm in diameter, 0.5 mm in thickness) were prepared by hot pressing as previously described. These pellets were placed into a 15 mm × 50 mm vial with a small stir bar, and 2 mL of a corresponding solvent was added into the vial. Samples were stirred at 250 rpm for up to 7 days unless the solution turned cloudy and the pellet inside fully dissolved. All solids and liquids were then transferred into a 35 mm × 16 mm dish to photograph the pellets or dispersions.

UV Masking of PHMA UV-XNP Films: PHMA UV-XNP films were masked with a UV-resistant adhesive vinyl film with a thickness of 0.1 mm. Masks of arbitrary shapes were cut using a Cricut Joy cutting machine. The specific design of masks and their respective curing methods are presented in the supporting information (Figure S20, Supporting Information). ≈0.2 mm PHMA UV-XNP films were cut into rectangular strips (50 mm × 5 mm for Figure 4A to C, or 60 mm × 7.5 mm for Figure 4D), covered with the masking film, and crosslinked without flipping. After removing the masking film, any residual adhesive on the samples was wiped off with methanol, a non-solvent for PHMA UV-XNPs.

Photoelastic Analysis: A photoelastic stress analysis setup was prepared on an Imada MX2-110 motorized test stand equipped with a ZTA-110 digital force gauge, and serrated screw grips with an initial grip separation of 30 mm (Figure 4A to C) or 40 mm (Figure 4D). A white LED panel coated with an adhesive polarization film was mounted at an angle of 45° to the direction of strain and was positioned behind the sample. A digital camera (RICOH GR IIIx) mounted on a tripod was placed in front of the sample, and the lens was covered with a polarizing filter perpendicular to the polarizing film on the LED panel. Samples were elongated at 50% strain per minute while recording with the digital camera. Samples in non-polarized lighting were photographed by removing the filter on the lens of a camera.

Demonstration of Stiffness-Patterned Soft Electronic Substrate: Approximately 0.2 mm thick PHMA UV-XNP films were cut into rectangular strips (70 mm × 10 mm). A 15 mm width section at the middle of the strip was irradiated with UV light for 9 h while the other areas of the strip were masked. A micro-LED with ≈10 mm long leads bent in parallel to the substrate adhered to the crosslinked domain using an epoxy adhesive. Starting from each end of the lead, a ≈3 mm wide line of eutectic gallium-indium was drawn on the substrate. The lines of liquid metal were connected to small pieces of copper tape adhered to each end of the UV-XNP substrate, and power was supplied to the electrical circuit using alligator clipping wires and a 9 V battery.

Demonstration of Component-Oriented Crosslinkable Soft Electronic Substrate: Approximately 0.2 mm thick PHMA UV-XNP films were cut into a rectangular shape (60 mm × 15 mm). Micro-LED chips (3.2 mm × 2.8 mm) were adhered to an arbitrary position using an epoxy adhesive. Then, a masking film with ovular cutouts (8 mm × 5 mm) where the center of the LED chips is located was designed and then was cut by the cutting machine. The UV-XNP substrate was flipped, and the UV mask was applied to the substrate on the backside to avoid blocking UV light to the substrate. These masked substrates were irradiated to UV light for 1 h. After the crosslinking, the mask was removed, and a ≈3 mm wide line of eutectic gallium-indium was drawn on the substrate. The lines of liquid metal were connected to small pieces of copper tape adhered to each end of the UV-XNP substrate, and power was supplied to the circuit using alligator clips and a 6 V battery.

Demonstration of Customizable Sensing Device: Approximately 0.2 mm thick PHMA UV-XNP film in an ≈8 mm diameter was used as feedstock. These films were combined into a wider film, if necessary, by hot pressing. Before the device fabrication, the master blueprint of the device was designed (Figure S23, Supporting Information). Based on this layout, the film was wrapped around the user's finger, and a rough outline was drawn using a permanent marker. Additionally, the position of electrical components was roughly tested using double-sided adhesive tape. Then, the UV-XNP film was cut into the drawn shape, and any residual ink from the maker was removed with methanol. The device components were adhered to the designated position using an epoxy adhesive. The customized masking film for the device was designed, cut by a cutting machine, and applied to the back of the device. The device was flipped and irradiated under UV light for 1 h. Then, a masking stencil was attached to the front of the substrate and used to draw the liquid metal wires (≈1 mm thick). At the ends of the device, two thin metal wires were adhered using epoxy adhesive, which were connected to the liquid metal wire. The fabricated device was mounted onto the user's finger using double-sided adhesive tape. Power was supplied to the device using the thin wires fixed on the back of the device and a 6 V battery. For additional crosslinking steps, a 0.5 mm thick shim supported the film to prevent damage of pre-drawn liquid metal. Informed written consent was obtained from participants in the experiments.

Supporting Information

Supporting Information is available from the Wiley Online Library or from the author.

Acknowledgements

This work was supported by the NSF via Award DMR-2204222. It was also supported by funding from the U.S. Army Research Office under ARO Award W911NF-22-1-0215. This work was carried out in part through the use of MIT.nano Characterization Facilities and equipment of Institute for Soldier Nanotechnologies, a U.S. Army-sponsored UARC at MIT. This work made use of MRSEC Shared Experimental Facilities at MIT, supported by the NSF under award DMR 14-19807.

Open access funding enabled and organized by MIT Hybrid 2025.

Conflict of Interest

The authors declare no conflict of interest.

Data Availability Statement

The data that support the findings of this study are available from the corresponding author upon reasonable request.

Keywords

composites, nanoparticles, photocrosslinking, polymers, processing

Received: July 19, 2024
Revised: December 30, 2024
Published online: January 28, 2025

[1] D. Nepal, S. Kang, K. M. Adstedt, K. Kanhaiya, M. R. Bockstaller, L. C. Brinson, M. J. Buehler, P. V. Coveney, K. Dayal, J. A. El-Awady, L. C. Henderson, D. L. Kaplan, S. Keten, N. A. Kotov, G. C. Schatz, S. Vignolini, F. Vollrath, Y. Wang, B. I. Yakobson, V. V. Tsukruk, H. Heinz, *Nat. Mater.* **2023**, *22*, 18.
[2] W. Cui, W. You, W. Yu, *Macromolecules* **2021**, *54*, 824.
[3] M. Malaki, R. S. Varma, *Adv. Mater.* **2020**, *32*, 2003154.
[4] D. G. Papageorgiou, Z. Li, M. Liu, I. A. Kinloch, R. J. Young, *Nanoscale* **2020**, *12*, 2228.
[5] F. Barthelat, Z. Yin, M. J. Buehler, *Nat. Rev. Mater.* **2016**, *1*, 16007.
[6] H. Zou, S. Wu, J. Shen, *Chem. Rev.* **2008**, *108*, 3893.
[7] C. Lei, Z. Xie, K. Wu, Q. Fu, *Adv. Mater.* **2021**, *33*, 2103495.
[8] G. Bae, G.-M. Choi, C. Ahn, S.-M. Kim, W. Kim, Y. Choi, D. Park, D. Jang, J.-W. Hong, S. M. Han, B.-S. Bae, S. Jeon, *Adv. Funct. Mater.* **2021**, *31*, 2010254.
[9] F. Lossada, D. Hoenders, J. Guo, D. Jiao, A. Walther, *Acc. Chem. Res.* **2020**, *53*, 2622.
[10] W. Huang, D. Restrepo, J.-Y. Jung, F. Y. Su, Z. Liu, R. O. Ritchie, J. McKittrick, P. Zavattieri, D. Kisailus, *Adv. Mater.* **2019**, *31*, 1901561.
[11] S. Wan, Q. Cheng, *Adv. Funct. Mater.* **2017**, *27*, 1703459.
[12] L. S. Dimas, G. H. Bratzel, I. Eylon, M. J. Buehler, *Adv. Funct. Mater.* **2013**, *23*, 4629.
[13] Y. Wen, C. Chen, Y. Ye, Z. Xue, H. Liu, X. Zhou, Y. Zhang, D. Li, X. Xie, Y.-W. Mai, *Adv. Mater.* **2022**, *34*, 2201023.
[14] H. Chen, V. V. Ginzburg, J. Yang, Y. Yang, W. Liu, Y. Huang, L. Du, B. Chen, *Prog. Polym. Sci.* **2016**, *59*, 41.
[15] S. Choi, S. Ihn Han, D. Kim, T. Hyeon, D.-H. Kim, *Chem. Soc. Rev.* **2019**, *48*, 1566.
[16] D.-P. Song, C. Li, W. Li, J. J. Watkins, *ACS Nano* **2016**, *10*, 1216.
[17] B. Li, P. I. Xidas, E. Manias, *ACS Appl. Nano Mater* **2018**, *1*, 3520.
[18] N. Yousefi, X. Sun, X. Lin, X. Shen, J. Jia, B. Zhang, B. Tang, M. Chan, J.-K. Kim, *Adv. Mater.* **2014**, *26*, 5480.
[19] Y. Fang, X. Yang, Y. Lin, J. Shi, A. Prominski, C. Clayton, E. Ostroff, B. Tian, *Chem. Rev.* **2022**, *122*, 5233.
[20] J. Huang, J. Zhou, M. Liu, *JACS Au* **2022**, *2*, 280.
[21] J. Loste, J.-M. Lopez-Cuesta, L. Billon, H. Garay, M. Save, *Prog. Polym. Sci.* **2019**, *89*, 133.
[22] T. Hueckel, X. Luo, O. F. Aly, R. J. Macfarlane, *Acc. Chem. Res.* **2023**, *56*, 1931.
[23] H. He, X. Shen, Z. Nie, *Prog. Polym. Sci.* **2023**, *143*, 101710.
[24] S. K. Kumar, N. Jouault, B. Benicewicz, T. Neely, *Macromolecules* **2013**, *46*, 3199.
[25] S. Askar, L. Li, J. M. Torkelson, *Macromolecules* **2017**, *50*, 1589.
[26] D. Maillard, S. K. Kumar, B. Fragneaud, J. W. Kysar, A. Rungta, B. C. Benicewicz, H. Deng, L. C. Brinson, J. F. Douglas, *Nano Lett.* **2012**, *12*, 3909.
[27] Y. Zhao, H. Wu, R. Yin, C. Yu, K. Matyjaszewski, M. R. Bockstaller, *Chem. Mater.* **2023**, *35*, 6990.
[28] Y. Zhao, Z. Wang, C. Yu, H. Wu, M. Olszewski, R. Yin, Y. Zhai, T. Liu, A. Coronado, K. Matyjaszewski, M. R. Bockstaller, *Macromolecules* **2022**, *55*, 8846.
[29] N. K. Hansoge, A. Gupta, H. White, A. Giuntoli, S. Keten, *Macromolecules* **2021**, *54*, 3052.
[30] J. M. Kubiak, B. Li, M. Suazo, R. J. Macfarlane, *ACS Appl. Mater. Interfaces* **2022**, *14*, 21535.
[31] Z. Wang, H. Chen, Y. Wang, J. Chen, M. A. Arnould, B. Hu, I. Popovs, S. M. Mahurin, S. Dai, *ACS Appl. Mater. Interfaces* **2021**, *13*, 27411.
[32] Z. Wang, Z. Lu, C. Mahoney, J. Yan, R. Ferebee, D. Luo, K. Matyjaszewski, M. R. Bockstaller, *ACS Appl. Mater. Interfaces* **2017**, *9*, 7515.
[33] F. Jiang, Y. Zhang, Z. Wang, W. Wang, Z. Xu, Z. Wang, *ACS Appl. Mater. Interfaces* **2015**, *7*, 10563.
[34] M. Moinuddin, M. Tripathy, *Macromolecules* **2022**, *55*, 9312.
[35] J. Midya, Y. Cang, S. A. Egorov, K. Matyjaszewski, M. R. Bockstaller, A. Nikoubashman, G. Fytas, *Nano Lett.* **2019**, *19*, 2715.
[36] M. Schmitt, J. Choi, C. M. Hui, B. Chen, E. Korkmaz, J. Yan, S. Margel, O. B. Ozdoganlar, K. Matyjaszewski, M. R. Bockstaller, *Soft Matter* **2016**, *12*, 3527.
[37] A. Agrawal, H.-Y. Yu, A. Sagar, S. Choudhury, L. A. Archer, *Macromolecules* **2016**, *49*, 8738.
[38] J. Choi, C. M. Hui, J. Pietrasik, H. Dong, K. Matyjaszewski, M. R. Bockstaller, *Soft Matter* **2012**, *8*, 4072.
[39] J. M. Kubiak, R. J. Macfarlane, *Adv. Funct. Mater.* **2022**, *32*, 2107139.
[40] J. M. Kubiak, R. J. Macfarlane, *Adv. Funct. Mater.* **2019**, *29*, 1905168.
[41] M. Kim, S. Hong, J. J. Park, Y. Jung, S. H. Choi, C. Cho, I. Ha, P. Won, C. Majidi, S. H. Ko, *Adv. Mater.* **2024**, *36*, 2313344.
[42] J. Ma, X. Huo, J. Yin, S. Cai, K. Pang, Y. Liu, C. Gao, Z. Xu, *Adv. Mater.* **2023**, *35*, 2305615.
[43] S. Huang, S. M. Adelmund, P. S. Pichumani, J. J. Schwartz, Y. Mengüç, M. Shusteff, T. J. Wallin, *Matter* **2023**, *6*, 2419.
[44] X. He, J. Cheng, Z. Li, H. Ye, X. Wei, H. Li, R. Wang, Y.-F. Zhang, H. Y. Yang, C. Guo, Q. Ge, *ACS Appl. Mater. Interfaces* **2023**, *15*, 3455.
[45] M. Takakuwa, K. Fukuda, T. Yokota, D. Inoue, D. Hashizume, S. Umezu, T. Someya, *Sci. Adv.* **2021**, *7*, eabl6228.
[46] X. Zhao, X. Chen, H. Yuk, S. Lin, X. Liu, G. Parada, *Chem. Rev.* **2021**, *121*, 4309.
[47] Q. Ge, Z. Chen, J. Cheng, B. Zhang, Y.-F. Zhang, H. Li, X. He, C. Yuan, J. Liu, S. Magdassi, S. Qu, *Sci. Adv.* **2021**, *7*, eaba4261.
[48] Y. Zheng, G.-J. N. Wang, J. Kang, M. Nikolka, H.-C. Wu, H. Tran, S. Zhang, H. Yan, H. Chen, P. Y. Yuen, J. Mun, R. H. Dauskardt, I. McCulloch, J. B.-H. Tok, X. Gu, Z. Bao, *Adv. Funct. Mater.* **2019**, *29*, 1905340.

[49] K. Chen, L. Zhang, X. Kuang, V. Li, M. Lei, G. Kang, Z. L. Wang, H. J. Qi, *Adv. Funct. Mater.* **2019**, *29*, 1903568.
[50] M. Kim, J. J. Park, C. Cho, S. H. Ko, *Adv. Funct. Mater.* **2023**, *33*, 2303286.
[51] H. Cho, B. Lee, D. Jang, J. Yoon, S. Chung, Y. Hong, *Mater. Horiz.* **2022**, *9*, 2053.
[52] J. Byun, B. Lee, E. Oh, H. Kim, S. Kim, S. Lee, Y. Hong, *Sci. Rep.* **2017**, *7*, 45328.
[53] S. K. Christensen, M. C. Chiappelli, R. C. Hayward, *Macromolecules* **2012**, *45*, 5237.
[54] J. Li, C. L. Lewis, D. L. Chen, M. Anthamatten, *Macromolecules* **2011**, *44*, 5336.
[55] S. Mukherjee, R. Xie, V. G. Reynolds, T. Uchiyama, A. E. Levi, E. Valois, H. Wang, M. L. Chabinyc, C. M. Bates, *Macromolecules* **2020**, *53*, 1090.
[56] R. Xie, S. Mukherjee, A. E. Levi, V. G. Reynolds, H. Wang, M. L. Chabinyc, C. M. Bates, *Sci. Adv.* **2020**, *6*, eabc6900.
[57] K. Matyjaszewski, H. Dong, W. Jakubowski, J. Pietrasik, A. Kusumo, *Langmuir* **2007**, *23*, 4528.
[58] J. O. Zoppe, N. C. Ataman, P. Mocny, J. Wang, J. Moraes, H.-A. Klok, *Chem. Rev.* **2017**, *117*, 1105.
[59] E. Dudognon, A. Bernès, C. Lacabanne, *Macromolecules* **2002**, *35*, 5927.
[60] S. Nanjundan, C. S. Unnithan, C. S. J. Selvamalar, A. Penlidis, *React. Funct. Polym.* **2005**, *62*, 11.
[61] F. W. Deeg, J. Pinsl, C. Braeuchle, *J. Phys. Chem.* **1986**, *90*, 5715.
[62] G. Desroches, Y. Wang, J. Kubiak, R. Macfarlane, *ACS Appl. Mater. Interfaces* **2022**, *14*, 9579.
[63] Y. Jiao, A. Tibbits, A. Gillman, M.-S. Hsiao, P. Buskohl, L. F. Drummy, R. A. Vaia, *Macromolecules* **2018**, *51*, 7257.
[64] F. Fleischhaker, A. P. Haehnel, A. M. Misske, M. Blanchot, S. Haremza, C. Barner-Kowollik, *Macromol. Chem. Phys.* **2014**, *215*, 1192.
[65] T. Çaykara, C. Özyürek, Ö. Kantoğlu, B. Erdoğan, *Polym. Degrad. Stab.* **2003**, *80*, 339.
[66] J. W. Dally, W. F. Riley, *Experimental Stress Analysis*, McGraw-Hill, New York, **1991**.
[67] L. M. Cox, A. K. Blevins, J. A. Drisko, Y. Qi, Y. Ding, C. I. Fiedler-Higgins, R. Long, C. N. Bowman, J. P. Killgore, *Adv. Eng. Mater.* **2019**, *21*, 1900578.
[68] N. D. Dolinski, Z. A. Page, E. B. Callaway, F. Eisenreich, R. V. Garcia, R. Chavez, D. P. Bothman, S. Hecht, F. W. Zok, C. J. Hawker, *Adv. Mater.* **2018**, *30*, 1800364.
[69] N. W. Bartlett, M. T. Tolley, J. T. B. Overvelde, J. C. Weaver, B. Mosadegh, K. Bertoldi, G. M. Whitesides, R. J. Wood, *Science* **2015**, *349*, 161.